Available online at www.sciencedirect.com
SCIENCE DIRECT®
Journal of Sound and Vibration 276 (2004) 361–379
JOURNAL OF SOUND AND VIBRATION
www.elsevier.com/locate/jsvi

Non-linear dynamic interactions of a Jeffcott rotor with preloaded snubber ring

E.E. Pavlovskaia*, E.V. Karpenko, M. Wiercigroch

Centre for Applied Dynamics Research, School of Engineering and Physical Sciences, King's College, University of Aberdeen, Aberdeen AB24 3UE, UK

Received 3 February 2003; accepted 22 July 2003

Abstract

A two-degrees-of-freedom model of a Jeffcott rotor with a preloaded snubber ring subjected to out-of-balance excitation has been developed. The purely impact interactions have been investigated. The rotor makes intermittent contacts with the preloaded snubber ring and as a consequence it can be in one of five different contact regimes, which boundaries have been found analytically. The current location of the snubber ring has been determined using the principle of the minimum elastic energy in the snubber ring. Consequently a non-linear piecewise smooth dynamical system has been obtained and studied numerically. The results in form of bifurcation diagrams, phase portraits and Poincaré maps show significant differences for the cases with and without preloading.

1. Introduction

Complex rotor systems have wide industrial applications, such as aero engines, steam and gas turbines, turbogenerators, etc. Forced vibrations in these systems are usually caused by centrifugal forces due to rotor mass imbalance, and various transmission forces. Even if the rotor is well balanced, the balance may deteriorate with use. To prevent the housing from deterioration caused by the excessive amplitude vibrations the preloading of the stator is often introduced. The level of the preloading together with imbalance, stiffness and damping crucially effect the dynamic system behaviour.

A full understanding of dynamics of real rotor systems (like gas turbines) is difficult and sometimes impossible without first considering the behaviour of simple models. To study the

*Corresponding author. Fax: +44-1224-272-497.
E-mail address: e.pavlovskaia@eng.abdn.ac.uk (E.E. Pavlovskaia).

0022-460X/$ - see front matter
doi:10.1016/j.jsv.2003.07.033

rotor–stator interactions, two- [1–10] or four-degrees-of-freedom [11–13] Jeffcott rotor models and simple structures like a shaft with one or more bearings [14,15] are often used.

Unwanted contact between the rotating and stationary parts of a rotating machine, more commonly referred to as rub, is a serious problem that has been regularly identified as a primary mode of failure in rotating machinery [13]. Rub may typically be caused by mass imbalance, turbine or compressor blade failure, defective bearings and/or seals, or by rotor misalignment, either thermal or mechanical. Several different physical events may occur during a contact between the rotor and the stator: an impact, friction between the two contacting parts, and a significant increase in the stiffness of the rotating system whilst contact is maintained, to name just three. The behaviour of the system in this case is highly non-linear and responses may be chaotic.

Rotor–stator rub interactions in rotating assemblies have attracted great attention from researches [1,2,4,9–13,16,17]. Choy and Padovan [1] studied the transient response associated with rubbing between a bladed rotor and its housing. Muszynska and Goldman [2] showed that during the impact of a rotating shaft against a stationary element, such as in the rotor-to-stator rub case, not only the radial (straight impact) effects must be taken into consideration, but, due to rotation, also the tangential effects. For the rub-impact Jeffcott rotor system supported on oil film bearings Chu and Zhang [11] found out four different scenarios to and out of chaos, namely, periodic, quasi-periodic, intermittent and period doubling bifurcation routes. In reference [9] Zhang et al. indicated that the non-linear rub-impact interactions caused by the rotor imbalance change the stable periodic motion of the system to quasi-periodic and chaotic motion and introduce period-doubling and grazing bifurcations. The reliability of the rotor system with rubbing was investigated theoretically by Chu and Zhang [10]. Dai et al. [12,16] proved that it is useful to introduce stops to limit violent vibration of rotor–bearing systems and that the friction factor plays an important role in the performance of the stops. Edwards et al. [13] and Al-Bedoor [17] present the models for the torsional and lateral vibrations of imbalanced rotors that account for the rotor-to-stator rubbing.

Previous studies on rotor systems have also addressed many important scientific and technical issues regarding stability [3,6,18,19]. A few papers concern control of the dynamic responses using smart materials and structures [8,14]. Zeng and Wang [8] created the model of the electromagnetic balancing regulator allowing the non-contact electromagnetic force to drive the correction masses so as to generate a suitable correction weight. Vibration control of a rotor system by a disk type electrorheological damper was applied by Yao et al. [14] to a six-degrees-of-freedom shaft model. This study showed that a controllable damping can suppress the large amplitude vibrations and sudden unbalance responses. Spontaneous sidebanding was investigated by Ehrich [5].

Separate attention of the researchers was given to rotor–stator impacts, which were studied both in the presence of the friction between the contacting parts (see, for example, Ref. [20]), and without it [7,21–23]. Three different models have been used so far [13]: (i) classical restitution coefficient approach, (ii) non-elastic impact with a zero restitution coefficient, where the impact is followed by a sliding stage, and (iii) piecewise approach, with extra stiffness and damping terms included during the contact stage. Using the third approach under assumption of absence of the friction force Neilson and Barr [21] and Gonsalves et al. [7] showed a reasonable correlation between the experimental and numerical results for four- and two-degrees-of-freedom Jeffcott

rotor models. Gonsalves et al. [7] have also identified the existence of chaotic vibrations for a Jeffcott rotor purely due to impacts. The recent papers by Karpenko et al. [22,23] studying the same type of rotor–stator impact confirmed these findings and have also showed an existence of multiple attractors and fractal basins of attractions.

Despite a significant number of theoretical and experimental investigations conducted so far, one of the important characteristics such as the effect of preloading of a snubber ring on the dynamics of a Jeffcott rotor model, which is an additional source of non-linearity in the rotor–stator system, has not been properly addressed yet. Therefore in this paper, a mathematical model of a Jeffcott rotor with a preloaded snubber ring is developed and the resultant system dynamics is studied.

2. Physical model and equations of motion

2.1. Physical model

A two-degrees-of-freedom model of the rotor system with a preloaded snubber ring is shown in Fig. 1a. The excitation is provided by an out-of-balance rotating mass $m\rho$. During operation the rotor of mass M makes intermittent contact with the snubber ring. It is assumed that contact is non-impulsive and that the friction between the snubber ring and the rotor is neglected. Since the mass ratio between the snubber ring and the mass of the rotor is small (for existing experimental rig it is equal to $\sim 1/17$) and the ratio between the stiffnesses of the snubber ring and the rotor is large, it is assumed that the snubber ring itself is massless. The stiffness and the viscous damping of the snubber ring are equal to k_s and c_s. The stiffness and the damping of the rotor are, respectively, k_r and c_r. The springs supporting the snubber ring are preloaded by Δ_x in horizontal and Δ_y in vertical directions, respectively. There is a gap γ between the rotor and the snubber ring. Also in the initial position, the centre of the rotor is displaced from the centre of the snubber ring by the eccentricity vector $\boldsymbol{\varepsilon}$.

The system can operate in (a) no contact or (b) contact between the rotor and the snubber ring. In the latter case, existence of the preloading makes the dynamics of the system more complicated as the force acting from the snubber ring on the rotor depends on whether the displacement of the snubber ring exceeds the preloadings (in one or both directions) or not. Thus, the following unique regimes of the system motion can be distinguished:

I. No contact between rotor and snubber ring.
II. Contact between the rotor and the snubber ring, where the both displacements of the snubber ring are smaller than the preloadings, i.e., $|x_s| \leqslant \Delta_x$ and $|y_s| \leqslant \Delta_y$.
III. Contact between the rotor and the snubber ring, where the displacement of the snubber ring in the horizontal direction is larger than the preloading, $|x_s| > \Delta_x$, and in the vertical direction is smaller than preloading, $|y_s| \leqslant \Delta_y$.
IV. Contact between the rotor and the snubber ring, where the displacement of the snubber ring in the horizontal direction is smaller than the preloading, $|x_s| \leqslant \Delta_x$, and in the vertical direction is larger than preloading, $|y_s| > \Delta_y$.
V. Contact between the rotor and the snubber ring, where the displacements of the snubber ring are larger than the preloadings, i.e., $|x_s| > \Delta_x$ and $|y_s| > \Delta_y$.

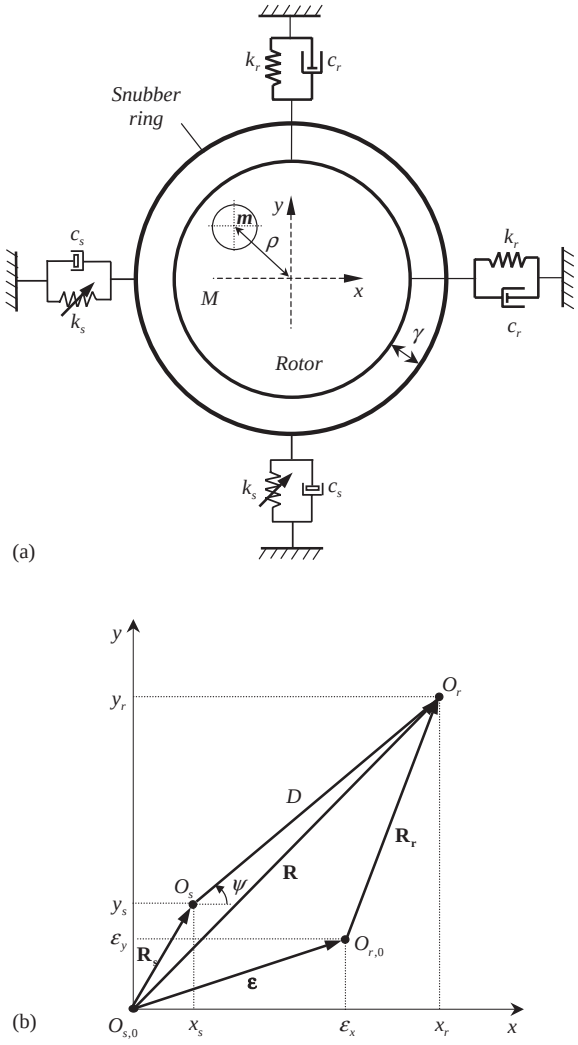

Fig. 1. (a) Physical model of the Jeffcott rotor with bearing clearance and (b) adopted co-ordinate system.

2.2. Equations of motion

The co-ordinate system adopted in this study is presented in Figs. 1b. The initial position of the rotor $O_{r,0}$ differs from the initial position of the snubber ring $O_{s,0}$ by the eccentricity vector $\boldsymbol{\varepsilon}$. The vectors $\mathbf{R}_r = (x_r, y_r)$ and $\mathbf{R}_s = (x_s, y_s)$ show the current positions of the rotor and the snubber ring, and $D = \sqrt{(x_r - x_s)^2 + (y_r - y_s)^2}$ is the distance between the centres of the rotor and the snubber ring at any given time. $R = \sqrt{x_r^2 + y_r^2}$ is the radial displacement of the rotor. For no contact situation the distance between the centres of the rotor and the snubber ring is smaller than the gap, γ, that is $D \leqslant \gamma$. Therefore, equations of motion for the rotor and the snubber

ring are

$$M\ddot{x}_r + c_r\dot{x}_r + k_r(x_r - \varepsilon_x) = m\rho\Omega^2\cos(\varphi_0 + \Omega t),$$
$$M\ddot{y}_r + c_r\dot{y}_r + k_r(y_r - \varepsilon_y) = m\rho\Omega^2\sin(\varphi_0 + \Omega t),$$
$$k_s x_s + c_s\dot{x}_s = 0, \quad k_s y_s + c_s\dot{y}_s = 0, \tag{1}$$

where φ_0 is the initial phase shift and Ω is shaft rotational velocity.

Once $D = \gamma$, the rotor hits the snubber ring and one or more of the contact regimes may occur, for which the equations of motion can be written as

$$M\ddot{x}_r + c_r\dot{x}_r + k_r(x_r - \varepsilon_x) + F_{s_x} = m\rho\Omega^2\cos(\varphi_0 + \Omega t),$$
$$M\ddot{y}_r + c_r\dot{y}_r + k_r(y_r - \varepsilon_y) + F_{s_y} = m\rho\Omega^2\sin(\varphi_0 + \Omega t),$$
$$x_s = x_s(x_r, y_r), \quad y_s = y_s(x_r, y_r). \tag{2}$$

Here the force in the snubber ring $\mathbf{F}_s = (F_{s_x}, F_{s_y})$ (see Fig. 2) varies for different contact regimes and will be determined in the next section. The unknown $x_s(x_r, y_r)$ and $y_s(x_r, y_r)$ give the current location of the snubber ring as a function of the current location of the rotor. To determine these functions the principle of minimum elastic energy of the snubber ring is used and a detailed analysis is also given in Section 3.

During any contact regime the distance between the centres of the rotor and the snubber ring remains constant, $D = \gamma$ despite of the fact that the force in the snubber ring, $\mathbf{F}_s$ may vary. In order to find the moment when the contact is lost the force $\mathbf{F}_s$ should be monitored. If the projection of this force $\mathbf{F}_s$ on the normal vector $\mathbf{n}$ to the surface of contact is positive (see Fig. 2), it is assumed that the rotor and the snubber ring are still in contact. Thus the contact is lost when

$$\mathbf{n}\cdot\mathbf{F}_s < 0 \quad \text{or} \quad \cos(\varphi - \psi) < 0, \tag{3}$$

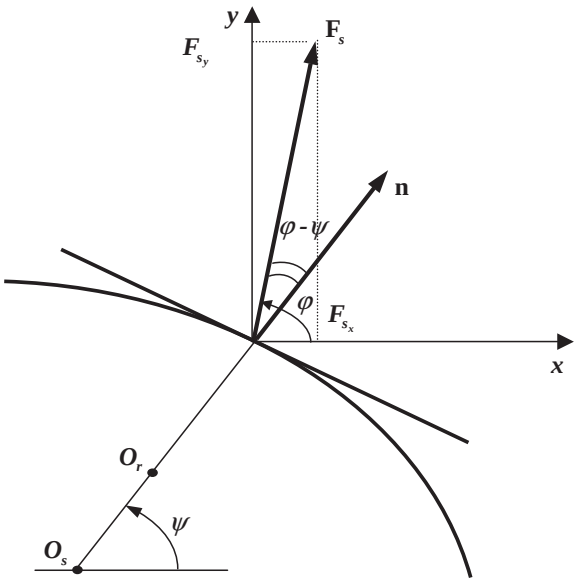

Fig. 2. Position of the force in the snubber ring $\mathbf{F}_s$ relative to the normal vector to the surface of contact.

where

$$\psi = \arccos\left(\frac{(x_r - x_s)}{\sqrt{(x_r - x_s)^2 + (y_r - y_s)^2}}\right), \quad \varphi = \arctan(F_{s_y}/F_{s_x}).$$

2.3. Non-dimensionalized equations of motion

In order to operate in the non-dimensional domain the following non-dimensional variables

$$\tau = \omega_n t, \quad \mathbf{f}_s = \mathbf{F}_s/(k_r\gamma), \quad \hat{x}_r = x_r/\gamma, \quad \hat{y}_r = y_r/\gamma, \quad \hat{x}_s = x_s/\gamma, \quad \hat{y}_s = y_s/\gamma, \quad v_{x_s} = \hat{x}_s'$$

and parameters

$$\eta = \Omega/\omega_n, \quad v_1 = c_r/(2\sqrt{k_r M}), \quad v_2 = c_s/(2\sqrt{k_r M}), \quad \eta_m = m/M, \quad \hat{\rho} = \rho/\gamma,$$
$$\hat{K} = k_s/k_r, \quad \hat{\varepsilon}_x = \varepsilon_x/\gamma, \quad \hat{\varepsilon}_y = \varepsilon_y/\gamma, \quad \hat{\Delta}_x = \Delta_x/\gamma, \quad \hat{\Delta}_y = \Delta_y/\gamma$$

are introduced. In addition, the non-dimensionalized restoring forces and radial displacements are defined as

$$\hat{F}_{rx} = F_{rx}/(k_r\gamma), \quad \hat{F}_{ry} = F_{ry}/(k_r\gamma), \quad \hat{F}_r = \sqrt{F_{rx}^2 + F_{ry}^2}/(k_r\gamma), \quad \hat{R} = R/\gamma.$$

Thus, equations of motion (1), (2) can be rewritten, and for the freely rotating rotor the equations of motion are

$$\begin{aligned}
&\hat{x}_r'' + 2v_1\,\hat{x}_r' + \hat{x}_r - \hat{\varepsilon}_x = \eta_m\hat{\rho}\,\eta^2\cos(\varphi_0 + \eta\tau),\\
&\hat{y}_r'' + 2v_1\,\hat{y}_r' + \hat{y}_r - \hat{\varepsilon}_y = \eta_m\hat{\rho}\,\eta^2\sin(\varphi_0 + \eta\tau),\\
&2v_2\hat{x}_s' + \hat{K}\hat{x}_s = 0, \quad 2v_2\hat{y}_s' + \hat{K}\hat{y}_s = 0.
\end{aligned} \tag{4}$$

For the regimes when the rotor is in contact with the snubber ring one has

$$\begin{aligned}
&\hat{x}_r'' + v_1\hat{x}_r' + \hat{x}_r - \hat{\varepsilon}_x + f_{s_x} = \eta_m\hat{\rho}\,\eta^2\cos(\varphi_0 + \eta\tau),\\
&\hat{y}_r'' + v_1\hat{y}_r' + \hat{y}_r - \hat{\varepsilon}_y + f_{s_y} = \eta_m\hat{\rho}\,\eta^2\sin(\varphi_0 + \eta\tau),\\
&\hat{x}_s = \hat{x}_s(\hat{x}_r, \hat{y}_r), \quad \hat{y}_s = \hat{y}_s(\hat{x}_r, \hat{y}_r),
\end{aligned} \tag{5}$$

where the differentiation with respect to non-dimensional time τ is denoted by prime.

3. Location of the snubber ring for contact regimes

3.1. Force in the snubber ring

It is assumed that the rotor and the snubber ring are in contact and the rotor moves the snubber ring in the direction shown in Fig. 3. The forces $\mathbf{F}_1$, $\mathbf{F}_2$, $\mathbf{F}_3$ and $\mathbf{F}_4$ generated in the snubber ring as a result of the rotor and the snubber ring interactions can be described in vector

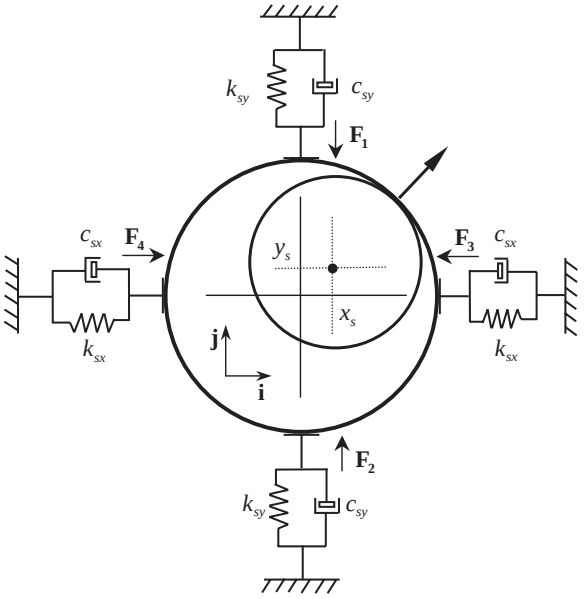

Fig. 3. Forces generated in the snubber ring.

form as

$$\mathbf{F}_1 = \begin{cases} -\mathbf{j}[k_s(\Delta_y + y_s) + c_s\dot{y}_s], & y_s > -\Delta_y, \\ \mathbf{0}, & y_s \leqslant -\Delta_y, \end{cases} \quad \mathbf{F}_2 = \begin{cases} \mathbf{j}[k_s(\Delta_y - y_s) - c_s\dot{y}_s], & y_s < \Delta_y, \\ \mathbf{0}, & y_s \geqslant \Delta_y, \end{cases}$$

$$\mathbf{F}_3 = \begin{cases} -\mathbf{i}[k_s(\Delta_x + x_s) + c_s\dot{x}_s], & x_s > -\Delta_x, \\ \mathbf{0}, & x_s \leqslant -\Delta_x, \end{cases} \quad \mathbf{F}_4 = \begin{cases} \mathbf{i}[k_s(\Delta_x - x_s) - c_s\dot{x}_s], & x_s < \Delta_x, \\ \mathbf{0}, & x_s \geqslant \Delta_x. \end{cases} \tag{6}$$

It is convenient to define the force in the snubber ring $\mathbf{F}_s$ as the resultant force taken with the opposite sign

$$\mathbf{F}_s = -(\mathbf{F}_1 + \mathbf{F}_2 + \mathbf{F}_3 + \mathbf{F}_4). \tag{7}$$

The values of this force are given in Table 1 for different regimes of operation. The expressions given above for $\mathbf{F}_s$ should be substituted to Eq. (2) to obtain equations of motion for different contact regimes and to Eq. (3) to determine the moment when the contact is lost.

3.2. Location of the snubber ring

When the rotor and the snubber ring are in contact, the distance between their centres remains constant and equal to the gap, so $(x_r - x_s)^2 + (y_r - y_s)^2 = \gamma^2$. In order to find the location of the snubber ring centre when it moves being in contact with the rotor, the following approach has been adopted. It is assumed that the snubber ring moving under the rotating rotor finds a position of minimum energy, E.

Table 1
Force in the snubber ring $\mathbf{F}_s$ for various regimes

$\mathbf{F}_s =$	Region
$\mathbf{i}[2k_s x_s + 2c_s\dot{x}_s] + \mathbf{j}[2k_s y_s + 2c_s\dot{y}_s]$	$\lvert x_s\rvert < \Delta_x,\ \lvert y_s\rvert < \Delta_y$
$\mathbf{i}[2k_s x_s + 2c_s\dot{x}_s] + \mathbf{j}[\mathrm{sign}(y_s)k_s(\Delta_y + \lvert y_s\rvert) + c_s\dot{y}_s]$	$\lvert x_s\rvert < \Delta_x,\ \lvert y_s\rvert \geqslant \Delta_y$
$\mathbf{i}[\mathrm{sign}(x_s)k_s(\Delta_x + \lvert x_s\rvert) + c_s\dot{x}_s] + \mathbf{j}[2k_s y_s + 2c_s\dot{y}_s]$	$\lvert x_s\rvert \geqslant \Delta_x,\ \lvert y_s\rvert < \Delta_y$
$\mathbf{i}[\mathrm{sign}(x_s)k_s(\Delta_x + \lvert x_s\rvert) + c_s\dot{x}_s] + \mathbf{j}[\mathrm{sign}(y_s)k_s(\Delta_y + \lvert y_s\rvert) + c_s\dot{y}_s]$	$\lvert x_s\rvert \geqslant \Delta_x,\ \lvert y_s\rvert \geqslant \Delta_y$

Table 2
Elastic energy of the snubber ring for various regimes

E	Region
$k_s x_s^2 + k_s y_s^2$	$\lvert x_s\rvert < \Delta_x,\ \lvert y_s\rvert < \Delta_y$
$(k_s/2)((\lvert x_s\rvert + \Delta_x)^2 - 2\Delta_x^2) + k_s y_s^2$	$\lvert x_s\rvert \geqslant \Delta_x,\ \lvert y_s\rvert < \Delta_y$
$k_s x_s^2 + (k_s/2)((\lvert y_s\rvert + \Delta_y)^2 - 2\Delta_y^2)$	$\lvert x_s\rvert < \Delta_x,\ \lvert y_s\rvert \geqslant \Delta_y$
$(k_s/2)((\lvert x_s\rvert + \Delta_x)^2 - 2\Delta_x^2) + (k_s/2)((\lvert y_s\rvert + \Delta_x)^2 - 2\Delta_y^2)$	$\lvert x_s\rvert \geqslant \Delta_x,\ \lvert y_s\rvert \geqslant \Delta_y$

The potential energy accumulated in the snubber ring at the position (x_s, y_s) is equal to the work, which is spent to bring the snubber ring to this position:

$$E = \int_{(s)} \mathbf{F}_s \, \mathrm{d}\mathbf{s} = -\int_0^{x_s} (\mathbf{F}_3 + \mathbf{F}_4)\mathbf{i} \, \mathrm{d}x_s - \int_0^{y_s} (\mathbf{F}_1 + \mathbf{F}_2)\mathbf{j} \, \mathrm{d}y_s. \tag{8}$$

Assuming that the work of viscous forces is negligible in comparison with the work of elastic forces, the expressions for the energy of the snubber ring take the forms listed in Table 2.

Then the problem of finding the current location of the snubber ring can be reduced to finding the minimum of the energy E with the constraint condition $D = \gamma$. This can be done using the Lagrange multipliers method by constructing the Lagrange function $L = E + \lambda\delta$, where λ is Lagrange multiplier, E is the elastic energy of the snubber ring, δ is the constraint function $\delta = (x_r - x_s)^2 + (y_r - y_s)^2 - \gamma^2$. As E and δ are the continuous and differentiable functions, the current position of the snubber ring (x_s and y_s) as a function of the current rotor position (x_r and y_r) can be determined from the conditions of the existence of extremum:

$$\partial L/\partial x_s = 0, \quad \partial L/\partial y_s = 0, \quad \partial L/\partial \lambda = \delta = 0, \tag{9}$$

where

$$L = E + \lambda((x_r - x_s)^2 + (y_r - y_s)^2 - \gamma^2).$$

Minimizing the energy E with the constraint $(x_r - x_s)^2 + (y_r - y_s)^2 = \gamma^2$, the functions $x_s(x_r, y_r)$ and $y_s(x_r, y_r)$ listed in Table 3 can be obtained.

Table 3
Functions $x_s(x_r, y_r)$ and $y_s(x_r, y_r)$ for various regimes of operation

$x_s = x_r\left(\sqrt{x_r^2 + y_r^2} - \gamma\right)/\sqrt{x_r^2 + y_r^2}$	$y_s = y_r\left(\sqrt{x_r^2 + y_r^2} - \gamma\right)/\sqrt{x_r^2 + y_r^2}$	$\lvert x_s\rvert < \Delta_x$, $\lvert y_s\rvert < \Delta_y$
$x_s = \mathrm{sign}(x_r)\left[\dfrac{2y_s(\lvert x_r\rvert + \Delta_x)}{y_r + y_s} - \Delta_x\right]$	$(y_r - y_s)^2((\lvert x_r\rvert + \Delta_x)^2 + (y_r + y_s)^2) = \gamma^2(y_r + y_s)^2$	$\lvert x_s\rvert \geqslant \Delta_x$, $\lvert y_s\rvert < \Delta_y$
$(x_r - x_s)^2((\lvert y_r\rvert + \Delta_y)^2 + (x_r + x_s)^2) = \gamma^2(x_r + x_s)^2$	$y_s = \mathrm{sign}(y_r)\left[\dfrac{2x_s(\lvert y_r\rvert + \Delta_y)}{x_r + x_s} - \Delta_y\right]$	$\lvert x_s\rvert < \Delta_x$, $\lvert y_s\rvert \geqslant \Delta_y$
$x_s = \mathrm{sign}(x_r)\left[\dfrac{(\lvert x_r\rvert + \Delta_x)(\tilde{R} - \gamma)}{\tilde{R}} - \Delta_x\right]$, $\tilde{R} = \sqrt{(\lvert x_r\rvert + \Delta_x)^2 + (\lvert y_r\rvert + \Delta_y)^2}$	$y_s = \mathrm{sign}(y_r)\left[\dfrac{(\lvert y_r\rvert + \Delta_y)(\tilde{R} - \gamma)}{\tilde{R}} - \Delta_y\right]$	$\lvert x_s\rvert \geqslant \Delta_x$, $\lvert y_s\rvert \geqslant \Delta_y$

3.3. Geometry of snubber ring location for contact regimes

Let us assume that the snubber ring has different stiffnesses in horizontal and vertical directions k_{sx} and k_{sy} and during the operation displacements of the snubber ring do not exceed the preloadings, $|x_s| \leqslant \Delta_x$ and $|y_s| \leqslant \Delta_y$. In this case the following geometrical interpretation of the snubber ring position under the moving rotor might be given.

Neglecting the dissipation of energy in the snubber ring one can rewrite the energy of the snubber ring as it was done earlier (see Table 2)

$$E = k_{sx}x_s^2 + k_{sy}y_s^2. \tag{10}$$

Thus for a chosen level of the energy E spent for moving the snubber ring, the equilibrium position of its centre (x_s, y_s) always belongs to an ellipse

$$x^2/(E/k_{sx}) + y^2/(E/k_{sy}) = 1. \tag{11}$$

On other hand, when the rotor and the snubber ring are in contact, the distance between the centres of the rotor and the snubber ring is equal to γ. If the current position of the rotor centre is (x_r, y_r), the equilibrium position of the snubber ring centre (x_s, y_s) can only belong to the circle

$$(x - x_r)^2 + (y - y_r)^2 = \gamma^2 \tag{12}$$

and this is shown in Fig. 4a. When the position of the centre of the rotor (x_r, y_r) is fixed, the corresponding position of the snubber ring can be viewed as the contact point between the ellipse (11) and the circle (12). The potential energy has its minimum when the ellipse touches the circle. The point of contact $O_s(x_s, y_s)$ between these curves can be found noting the ellipse and the circle sharing the same tangential, u. Since both functions for the ellipse (G_e) and the circle (G_c) are implicit, the tangentials can be calculated as

$$-(\partial G_i/\partial y)_{y=y_s}(y - y_s) = (\partial G_i/\partial x)_{x=x_s}(x - x_s), \tag{13}$$

where $i = e, c$. For the ellipse one has $G_e = k_{sx}x^2/E + k_{sy}y^2/E - 1$ and the tangential is

$$x_s(x - x_s)k_{sx} + y_s(y - y_s)k_{sy} = 0. \tag{14}$$

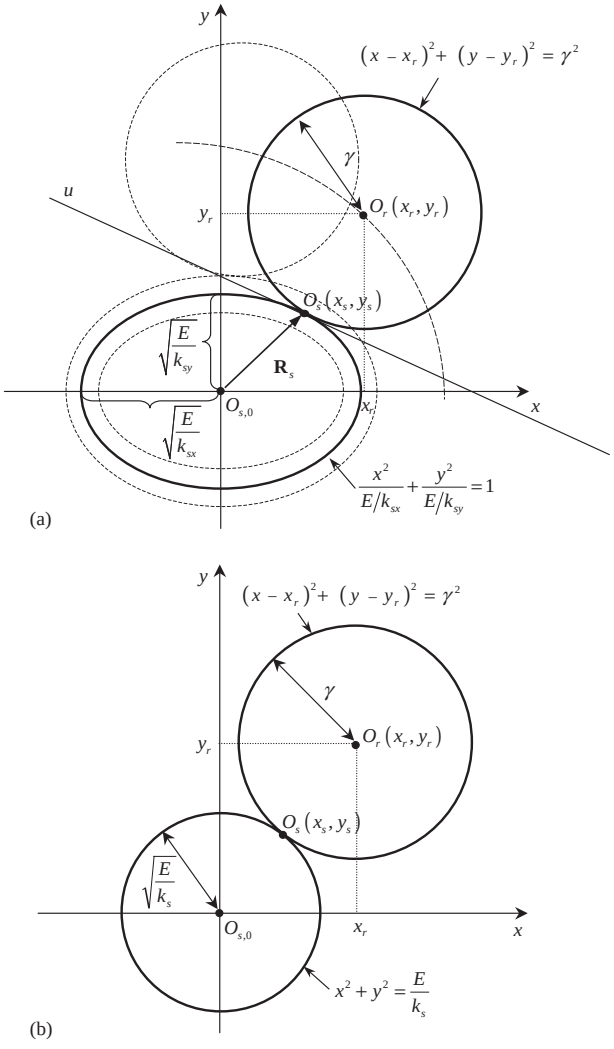

Fig. 4. Geometrical interpretation of the location of the snubber ring position: (a) for different stiffnesses of the snubber ring in the x and y directions, (b) for the same stiffnesses of the snubber ring in the x and y directions.

Eq. (14) can be rewritten in explicit form as

$$y = k_1(x_r, x_s, y_r, y_s)x + b_1(x_r, x_s, y_r, y_s). \tag{15}$$

For the circle $G_c = (x - x_r)^2 + (y - y_r)^2 - \gamma^2$ formula for the tangential is

$$(x_s - x_r)(x - x_s) + (y_s - y_r)(y - y_s) = 0 \tag{16}$$

or

$$y = k_2(x_r, x_s, y_r, y_s)x + b_2(x_r, x_s, y_r, y_s). \tag{17}$$

Equating the coefficients $k_1 = k_2$ and $b_1 = b_2$ and solving the obtained algebraic equations together with the condition of contact

$$(x_r - x_s)^2 + (y_r - y_s)^2 = \gamma^2 \tag{18}$$

the relationship between the rotor and the snubber ring positions can be written as

$$x_s = f_1(x_r, y_r), \quad y_s = f_2(x_r, y_r). \tag{19}$$

For a simple case when stiffnesses of the snubber ring are the same in both directions, $k_{sx} = k_{sy} = k_s$, the tangentials for the ellipse and the circle are

$$\begin{aligned} &y = -(x_s/y_s)x + (x_s^2 + y_s^2)/y_s, \\ &y = -(x_s - x_r)/(y_s - y_r)\, x + (x_s(x_s - x_r) + y_s(y_s - y_r))/(y_s - y_r). \end{aligned} \tag{20}$$

Equating the coefficients gives

$$x_s/x_r = y_s/y_r. \tag{21}$$

After substituting Eq. (21) into the condition of contact (18) finally one obtains:

$$x_s = x_r(1 - \gamma/\sqrt{x_r^2 + y_r^2}) = x_r(R - \gamma)/R, \quad y_s = y_r(1 - \gamma/\sqrt{x_r^2 + y_r^2}) = y_r(R - \gamma)/R. \tag{22}$$

In this case, the ellipse in Fig. 4a transforms to circle with the radius $\sqrt{E/k_s}$, as shown in Fig. 4b.

4. Contact regimes

Let one now consider the motion of the rotor in detail. As mentioned earlier the rotor can move either in or out of contact with the snubber ring. During the contact the force acting between the rotor and the snubber ring significantly depends on the "depth" of contact and four different regimes can occur as listed in Section 2. This can be clearly explained using (x_r, y_r) plane where each regime is mapped into an associated region as shown in Fig. 5. The boundaries between regimes I, II, III, IV and V are determined from the conditions listed at the top right quadrant at Fig. 5. The equations describing these boundaries were developed in Section 4 and graphically depicted in Fig. 6 which shows only one quadrant of (x_r, y_r) plane since the problem is symmetric. A detailed explanation how all these regions were determined is given below.

Region I, or no contact region is realized inside the circle

$$x_r^2 + y_r^2 = \gamma^2. \tag{23}$$

Once the rotor makes a contact with the snubber ring the contact regime II begins. The boundaries of the corresponding region on (x_r, y_r) plane can be specified as follows. The inner boundary is described by Eq. (23). The outer boundaries are governed by the conditions $|x_s| = \Delta_x$ and $|y_s| = \Delta_y$. Substituting x_s and y_s as function of x_r and y_r given in Table 3 for $|x_s| \leqslant \Delta_x$ and $|y_s| \leqslant \Delta_y$, in the first quadrant of (x_r, y_r) plane the outer boundaries are given by

$$y_r = \frac{x_r}{x_r - \Delta_x}\sqrt{\gamma^2 - (x_r - \Delta_x)^2}, \quad x_r = \frac{y_r}{y_r - \Delta_y}\sqrt{\gamma^2 - (y_r - \Delta_y)^2}. \tag{24, 25}$$

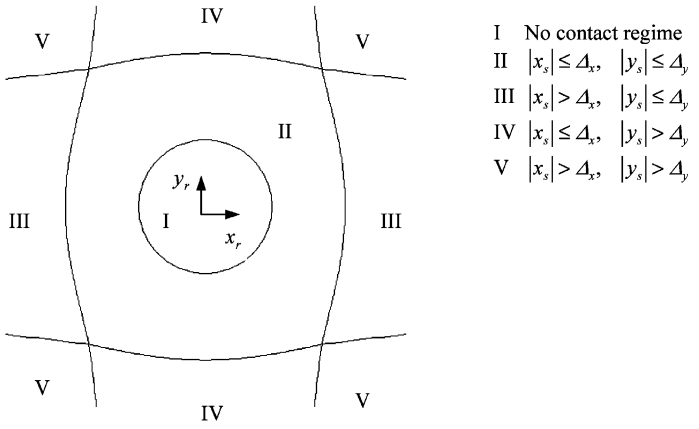

Fig. 5. Regions of operation for a rotor system with a symmetrically preloaded snubber ring in (x_r, y_r) plane.

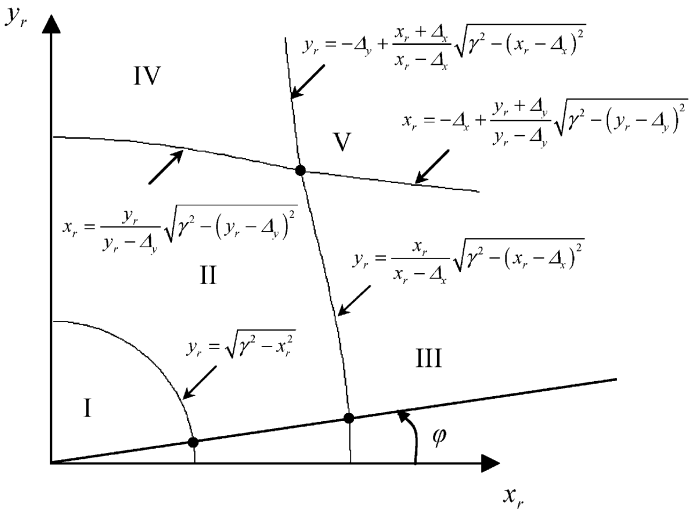

Fig. 6. Regions of operation and their boundaries for the first quadrant of (x_r, y_r) plane.

Once the rotor drags the snubber ring "deep" enough in the horizontal direction, i.e., its displacement, x_s becomes larger than the preloading Δ_x, the regime III begins. The inner (left) border for the region III is described by Eq. (24) and the outer (upper) border again is governed by the conditions $|y_s| = \Delta_y$. As this border is simultaneously the inner (lower) border for the region V, the explicit expression for y_s as function of x_r and y_r given in Table 3 for $|x_s| > \Delta_x$ and $|y_s| > \Delta_y$ is used

$$x_r = -\Delta_x + (y_r + \Delta_y)/(y_r - \Delta_y)\sqrt{\gamma^2 - (y_r - \Delta_y)^2}. \tag{26}$$

In the same way for the rotor moving during regime IV one can obtain that the inner (lower) border for the region IV is described by Eq. (25) and the outer (right) border is

$$y_r = -\Delta_y + (x_r + \Delta_x)/(x_r - \Delta_x)\sqrt{\gamma^2 - (x_r - \Delta_x)^2}. \tag{27}$$

Finally, the inner (and only) borders of the region V are described by Eqs. (26) and (27).

Now let introduce the elastic restoring force vector $\mathbf{F}_r = (F_{r_x}, F_{r_y})$ acting on the rotor. For no contact regime I, its components are equal to

$$F_{r_x} = k_r(x_r - \varepsilon_x), \quad F_{r_y} = k_r(y_r - \varepsilon_y) \tag{28}$$

and for contact regimes are described as

$$F_{r_x} = k_r(x_r - \varepsilon_x) + p_x k_s x_s, \quad F_{r_y} = k_r(y_r - \varepsilon_y) + p_y k_s y_s, \tag{29}$$

where

$$p_x = \left\{ \begin{array}{ll} 1, & \text{for regimes III, V} \\ 2, & \text{for regimes II, IV} \end{array} \right\}, \quad p_y = \left\{ \begin{array}{ll} 1, & \text{for regimes IV, V} \\ 2, & \text{for regimes II, III} \end{array} \right\}.$$

The components of the elastic restoring force F_{r_x}, F_{r_y} and $F_r = \sqrt{F_{r_x}^2 + F_{r_y}^2}$ as functions of x_r and y_r form 3D surfaces. In Figs. 7a–c these 3D surfaces are shown in non-dimensional co-ordinates (see Section 2.3). These surfaces are calculated for $\hat{\Delta}_x = 1.5$, $\hat{\Delta}_y = 1.1$ and $\hat{K} = 30$. As can be seen from these figures, there are well-pronounced borders between the different regions, which coincide with boundaries $\sqrt{\hat{x}_r^2 + \hat{y}_r^2} = 1$, $\hat{x}_s = \hat{\Delta}_x$ and $\hat{y}_s = \hat{\Delta}_y$, and the components of the elastic restoring force $\hat{F}_{r_x}$, $\hat{F}_{r_y}$ and $\hat{F}_r$ are changing when crossing these borders. In Fig. 7d the component of the restoring force $\hat{F}_{r_x}$ is plotted as a function of the radial displacement, $\hat{R} = \sqrt{\hat{x}_r^2 + \hat{y}_r^2}$ for three different values of angle $\varphi = \arctan(y_r/x_r)$ which meaning is shown in Fig. 6. The dot line corresponds to $\varphi = 27^\circ$, solid line to $\varphi = \arctan(\Delta_y/\Delta_x) = 66^\circ$ and dash line to $\varphi = 85^\circ$. For each value of φ there are two points on the curve at which the slop is changing. First of them is on the border between regions I and II ($\hat{R} = 1$), and it corresponds to the beginning of the contact regimes. The second point occurs when the value of the snubber ring displacement $\hat{x}_s$ exceeds the preloading $\hat{\Delta}_x$. As can be deduced from Fig. 6 for $\hat{F}_{r_x}$ this second point appears on the border between regions II and III for $\varphi < \arctan(\Delta_y/\Delta_x)$, on the border between regions II and V for $\varphi = \arctan(\Delta_y/\Delta_x)$, and on the border between phases IV and V for $\varphi > \arctan(\Delta_y/\Delta_x)$. As $\hat{F}_{r_x}$ does not depend on $\hat{y}_s$ there is no change in the curve slop when the value of the snubber ring displacement $\hat{y}_s$ exceeds the preloading $\hat{\Delta}_y$, i.e., on the borders between phases II and IV and between phases III and V. Similar explanations can be given for $\hat{F}_{r_y}$ and $\hat{F}_r$.

5. Numerical investigations

Numerical results presented in this section are to demonstrate the use of the developed analytical formulas and show the influence of the preloading on the dynamics of the rotor crossing different regions of operation.

Bifurcation diagrams shown in Fig. 8 were constructed for the displacement of the rotor $\hat{x}_r$ under varying the frequency ratio η for the unpreloaded (Fig. 8a) and the preloaded (Fig. 8b)

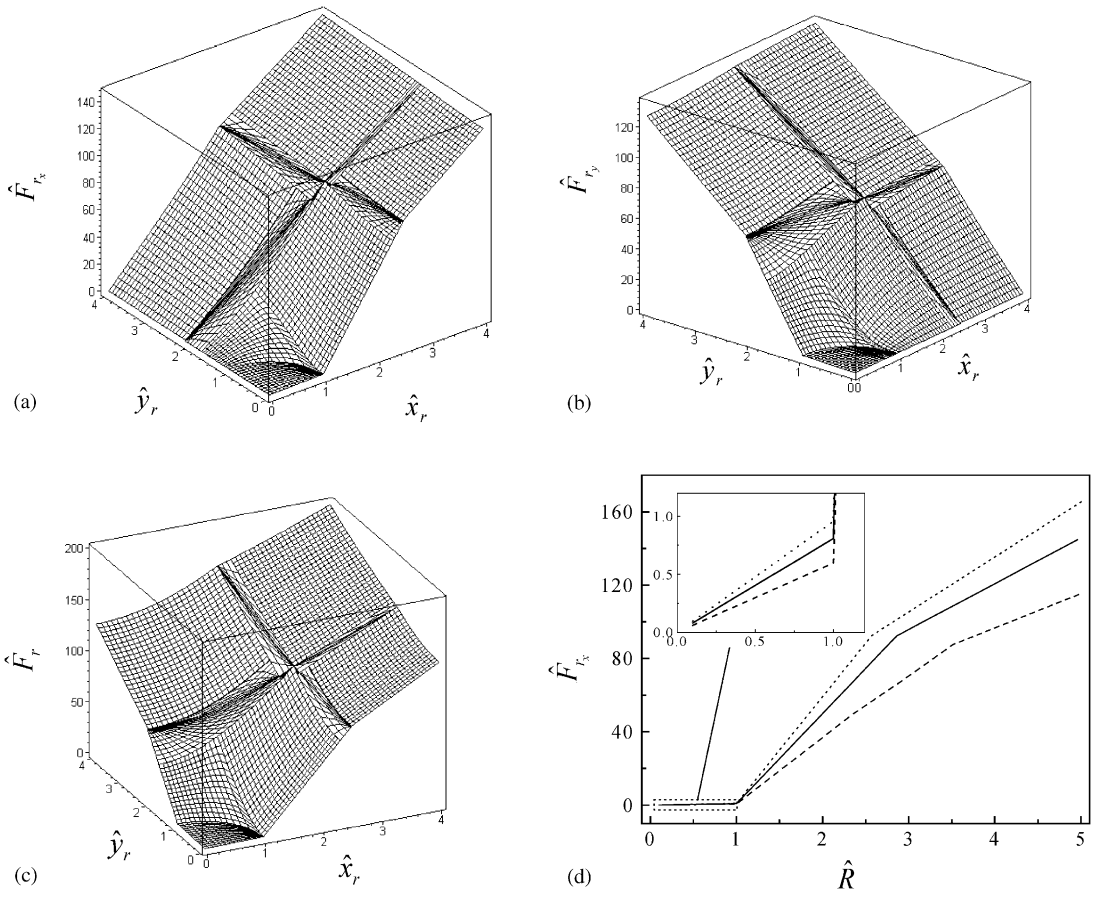

Fig. 7. (a), (b) and (c) Non-dimensionalized restoring forces $\hat{F}_{r_x}$, $\hat{F}_{r_y}$ and $\hat{F}_r$ as functions of x_r and y_r, calculated for $\hat{\Delta}_x = 1.5$, $\hat{\Delta}_y = 1.1$, $\hat{K} = 30$ and (d) restoring force $\hat{F}_{r_x}$ as function of radial displacement $\hat{R}$, where case $\varphi = \arctan(\hat{\Delta}_y/\hat{\Delta}_x)$ is marked by solid line, $\varphi > \arctan(\hat{\Delta}_y/\hat{\Delta}_x)$ by dash line and $\varphi < \arctan(\hat{\Delta}_y/\hat{\Delta}_x)$ by dotted line, respectively.

cases. The control parameter η was set to the leftmost value 2. Starting with zero initial conditions first 300 cycles were calculated without plotting anything to ensure that steady state solutions had been reached. The next 150 cycles produced values of the displacement $\hat{x}_r$, which were plotted. Then a small increment was added to the control parameter and the procedure was repeated until the control parameter reached the rightmost value, $\eta = 5$. The parameters used in numerical calculations were as follows: $v_1 = 0.125$, $v_1 = 0.002$, $\hat{K} = 30$, $\hat{\varepsilon}_x = 0.9$, $\hat{\varepsilon}_y = 0$, $\eta_m = 70$, $\hat{\rho} = 0.0017$. The preloading was set to zero in both directions for Fig. 8a, and $\hat{\Delta}_x = \hat{\Delta}_y = 0.1$ for Fig. 8b. As can be clearly seen from Fig. 8 the preloading significantly changes the bifurcation structure. First of all it shifts the existing bifurcation points; dash lines in Fig. 8 point out such behaviour. For instance the period one observed in the beginning of the diagram bifurcates at $\eta = 2.165$ for unpreloaded and at $\eta = 2.213$ for preloaded case. The point of bifurcation of period four motion into period two motion moves from $\eta = 2.717$ to 2.824, and the period two bifurcates into period four at $\eta = 3.803$ and 3.893 for unpreloaded and preloaded cases, respectively.

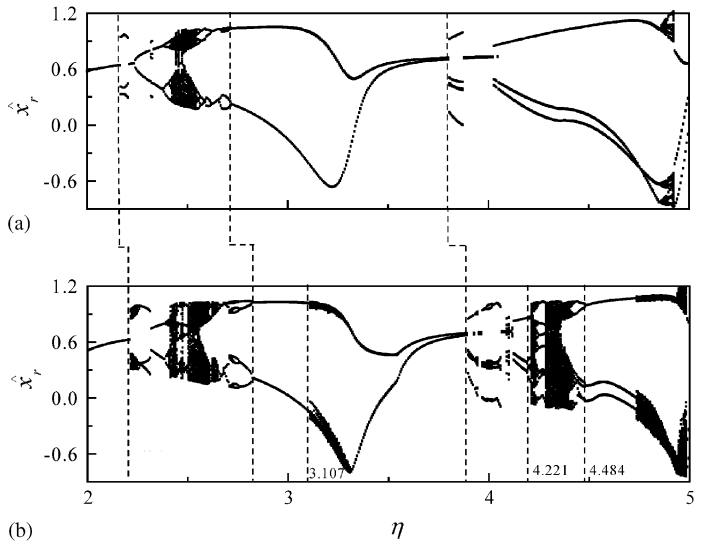

Fig. 8. Bifurcation diagrams $\hat{x}_r(\eta)$ calculated for (a) $\hat{\Delta}_x = \hat{\Delta}_y = 0$; (b) $\hat{\Delta}_x = \hat{\Delta}_y = 0.1$; and $v_1 = 0.125$, $v_2 = 0.002$, $\hat{K} = 30$, $\eta_m = 0.0017$, $\hat{\rho} = 70$, $\hat{\varepsilon}_x = 0.9$ and $\hat{\varepsilon}_y = 0$.

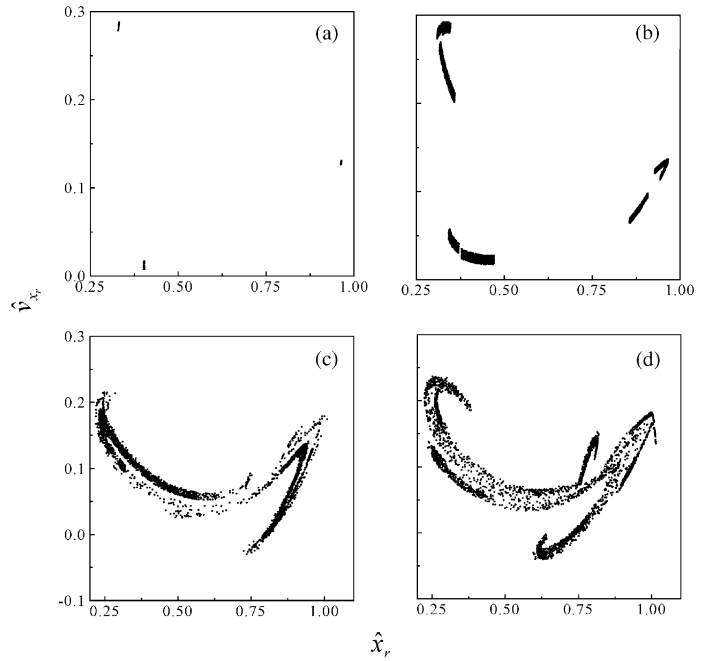

Fig. 9. Poincaré maps $\hat{v}_{x_r}(\hat{x}_r)$ calculated for (a), (c) $\hat{\Delta}_x = \hat{\Delta}_y = 0$; (b), (d) $\hat{\Delta}_x = \hat{\Delta}_y = 0.1$; $v_1 = 0.125$, $v_2 = 0.002$, $\hat{K} = 30$, $\eta_m = 0.0017$, $\hat{\rho} = 70$, $\hat{\varepsilon}_x = 0.9$ and $\hat{\varepsilon}_y = 0$; and (a) $\eta = 2.223$, (b) $\eta = 2.181$ and (c), (d) $\eta = 2.442$.

Secondly, the introduction of the preloading changes the character of bifurcations. For example, the period one motion marked the leftmost dash line, roughly speaking bifurcates into period three motion (see Poincaré map in Fig. 9a) for unpreloaded case and into quasi-periodic

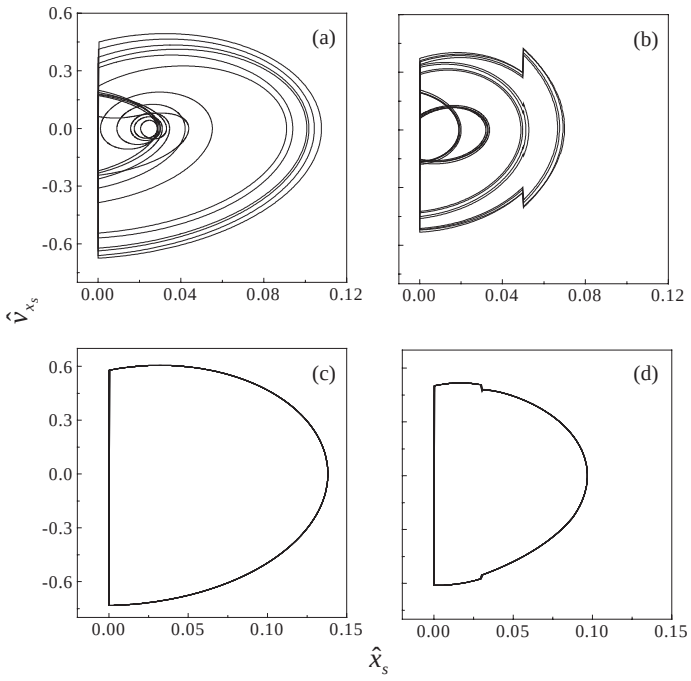

Fig. 10. Phase portraits $\hat{v}_{x_s}(\hat{x}_s)$ calculated for: (a) $\hat{\Delta}_x = \hat{\Delta}_y = 0$; (b) $\hat{\Delta}_x = \hat{\Delta}_y = 0.05$ and $v_1 = 0.06$, $v_2 = 0.002$, $\eta = 2.5$, $\hat{K} = 30$, $\hat{\varepsilon}_x = 0.4$, $\hat{\varepsilon}_y = 0.5$, $\rho = 70$, $\eta_m = 0.00289$; and for (c) $\hat{\Delta}_x = \hat{\Delta}_y = 0$; (d) $\hat{\Delta}_x = \hat{\Delta}_y = 0.03$ and $v_1 = 0.125$, $v_2 = 0.002$, $\eta = 3.0$, $\hat{K} = 30$, $\hat{\varepsilon}_x = 0.9$, $\hat{\varepsilon}_y = 0$, $\rho = 70$, $\eta_m = 0.0017$.

motion (Fig. 9b) for preloaded case. Also the preloading changes the structure of the chaotic attractor and this can be seen from Poincaré maps shown in Figs. 9c and d calculated at $\eta = 2.442$ for unpreloaded and preloaded cases.

Finally and most importantly the preloading introduces new bifurcations and new regimes. For example, an additional bifurcation of the period two motion into quasi-periodic motion appears at $\eta \approx 3.107$ for the preloaded case. Also a large window of new regimes containing periodic, quasi-periodic and chaotic motions arises between $\eta \approx 4.211$ and 4.484 where for unpreloaded case the only period three motion is observed.

The changes in dynamical behaviour are even more visible in $(\hat{x}_s, \hat{v}_{x_s})$ plane. The comparison between trajectories of the snubber ring on the phase plane $(\hat{x}_s, \hat{v}_{x_s})$ for the system with and without preloading is presented in Fig. 10. Dynamics of the snubber ring is shown in Figs. 10a and c for the system without preloading ($\hat{\Delta}_x = \hat{\Delta}_y = 0$), and in Figs. 10b and d for the system with preloading ($\hat{\Delta}_x = \hat{\Delta}_y = 0.05$ and 0.03, respectively). The values of other system parameters are also different for Figs. 10a–d and they are given in the figure caption. As can be seen from Fig. 10 in both cases, velocity of snubber ring $\hat{v}_{x_s}$ experiences a jump at $\hat{x}_s = 0$, when the rotor hits the snubber ring. For the systems with preloading there is an additional jump of velocity $\hat{v}_{x_s}$, which appears at $\hat{x}_s = \hat{\Delta}_x$. Also it can be observed that the existence of the preloading reduces the amplitude of the snubber ring vibrations.

6. Conclusions

Two-degrees-of-freedom model of the Jeffcott rotor with the preloaded snubber ring subjected to out-of-balance excitation was developed, and dynamic interactions between the rotor and the preloaded snubber ring were studied. During operation the rotor can be in one of five different contact regimes, for which boundaries on (x_r, y_r) plane have been analytically determined. The current location of the snubber ring has been obtained using the principle of the minimum elastic energy in the snubber ring. The equations of motion were solved numerically and the results of the calculations for the system with and without preloading were compared using bifurcation diagrams and phase portraits. It was shown that the introduction of the preloading significantly change the bifurcation structure, i.e., it shifts the existing bifurcation points, changes the character of the bifurcations and introduces new bifurcations and new regimes. The changes in dynamical behaviour are also clearly visible on the phase portraits of the system, where the preloading introduces additional jumps of the snubber ring velocities and changes the amplitude of the snubber ring vibrations.

Further numerical analysis reveals that the model is very sensitive for both the direction and the magnitude of the preloading. Accordingly it can be concluded that influence of the preloading on the dynamics of the Jeffcott rotor with preloaded ring is crucial and should be considered in the mathematical models.

Acknowledgements

The financial support provided by EPSRC, Rolls-Royce plc. and ORS award scheme is gratefully acknowledged.

Appendix A. Nomenclature

c_r	damping coefficient of the rotor
c_s	damping coefficient of the snubber ring
D	distance between the centres of the rotor and the snubber ring
E	elastic energy of the snubber ring
$\mathbf{F}_r = (F_{r_x}, F_{r_y})$	restoring force vector
$\mathbf{F}_s = (F_{s_x}, F_{s_y})$	force vector in the snubber ring
k_r	rotor stiffness
k_s	snubber ring stiffness
k_1, k_2, b_1, b_2	auxiliary coefficients
M	mass of rotor
$\mathbf{n}$	normal vector to the surface of contact
$m\rho$	out-of-balance
t	time
R	radial displacement of the rotor relative to the initial position of the snubber ring

$\mathbf{R}_r = (x_r, y_r)$	radius vector of the current position of the rotor, $\lvert\mathbf{R}_r\rvert = R$
$\mathbf{R}_s = (x_s, y_s)$	radius vector of the current position of the snubber ring
Δ_x, Δ_y	preloadings of the snubber ring in the horizontal and vertical directions
$\hat{K}$	stiffness ratio, k_s/k_r
$\hat{x}_r$, $\hat{y}_r$	non-dimensional horizontal and vertical co-ordinates of the current position of the rotor
$\hat{x}_s$, $\hat{y}_s$	non-dimensional horizontal and vertical co-ordinates of the current position of the snubber ring
$\hat{\Delta}_x$, $\hat{\Delta}_y$	non-dimensional preloadings of the snubber ring in horizontal and vertical directions
$\hat{R}$	non-dimensional radial displacement, R/γ
ε_x, ε_y	eccentricities of the rotor in x and y directions
φ_0	initial phase shift
γ	radial clearance between the rotor and the snubber ring
η	frequency ratio, Ω/ω_n
η_m	mass ratio, m/M
ν_1	damping ratio of the rotor, $c_r/(2\sqrt{k_r M}y)$
ν_2	damping ratio of the snubber ring, $c_s/(2\sqrt{k_r M}y)$
τ	non-dimensional time, $\omega_n t$
ψ	the angle between the normal to the surface of contact and the horizontal direction
ω_n	natural frequency of the rotor, $\sqrt{k_r/M}$
$\hat{\varepsilon}_x$	non-dimensional eccentricity in the x direction, ε_x/γ
$\hat{\varepsilon}_y$	non-dimensional eccentricity in the y direction, ε_y/γ
$\hat{\rho}$	non-dimensional radius, ρ/γ
Ω	shaft rotational velocity

References

[1] F.K. Choy, J. Padovan, Non-linear transient analysis of rotor-casing rub events, *Journal of Sound and Vibration* 113 (3) (1987) 529–545.

[2] A. Muszynska, P. Goldman, Chaotic responses of unbalanced rotor/bearing/stator systems with looseness or rubs, *Chaos, Solitons and Fractals* 5 (9) (1995) 1683–1704.

[3] R. Ganesan, Dynamic response and stability of a rotor-support system with non-symmetric bearing clearances, *Mechanism and Machine Theory* 31 (6) (1996) 781–798.

[4] D.W. Childs, Fractional-frequency rotor motion due to nonsymmetric clearance effects, *Transactions of the American Society of Mechanical Engineers, Journal of Engineering for Power* 104 (3) (1982) 533–541.

[5] F.F. Ehrich, Spontaneous sideband ing in high-speed rotordynamics, *Transactions of the American Society of Mechanical Engineers, Journal of Vibration and Acoustics* 114 (4) (1992) 498–505.

[6] G. von Groll, D.J. Ewins, The harmonic balance method with arc-length continuation in rotor/stator contact problems, *Journal of Sound and Vibration* 241 (2) (2001) 223–233.

[7] D.H. Gonsalves, R.D. Neilson, A.D.S. Barr, A study of the response of a discontinuously nonlinear rotor system, *Nonlinear Dynamics* 7 (1995) 451–470.

[8] S. Zeng, X.-X. Wang, The influence of the electromagnetic balancing regulator on the rotor system, *Journal of Sound and Vibration* 219 (4) (1999) 723–729.

[9] Y. Zhang, B. Wen, A. Leung, Reliability analysis for rotor rubbing, *Journal of Vibration and Acoustics* 124 (2002) 58–62.
[10] F. Chu, Z. Zhang, Bifurcation and chaos in a rub-impact Jeffcott rotor system, *Journal of Sound and Vibration* 210 (1) (1998) 1–18.
[11] F. Chu, Z. Zhang, Periodic quasi-periodic and chaotic vibrations of a rub-impact rotor system supported on oil film bearings, *International Journal of Engineering Science* 35 (10/11) (1997) 963–973.
[12] X. Dai, X. Zhang, X. Jin, The partial and full rubbing of a flywheel rotor–bearing–stop system, *International Journal of Mechanical Sciences* 43 (2001) 505–519.
[13] S. Edwards, A.W. Lees, M.I. Friswell, The influence of torsion on rotor/stator contact in rotating machinery, *Journal of Sound and Vibration* 225 (5) (1999) 767–778.
[14] G.Z. Yao, Y. Qiu, G. Meng, T. Fang, Y.B. Fan, Vibration control of a rotor system by disk type electrorheological damper, *Journal of Sound and Vibration* 219 (1) (1999) 175–188.
[15] M.A. Mohiuddin, M. Bettayeb, Y.A. Khulief, Dynamic analysis and reduced order modelling of flexible rotor–bearing system, *Computers and Structures* 69 (1998) 349–359.
[16] X. Dai, Z. Jin, X. Zhang, Dynamic behavior of the full rotor/stop rubbing: numerical simulation and experimental verification, *Journal of Sound and Vibration* 251 (5) (2002) 807–822.
[17] B.O. Al-Bedoor, Transient torsional and lateral vibrations of unbalanced rotors with rotor-to-stator rubbing, *Journal of Sound and Vibration* 229 (3) (2000) 627–645.
[18] Y.-B. Kim, S.T. Noah, Quasi-periodic response and stability analysis for a non-linear Jeffcott rotor, *Journal of Sound and Vibration* 190 (2) (1996) 239–253.
[19] A. Raghothama, S. Narayanan, Bifurcation and chaos in geared rotor bearing system by incremental harmonic balance method, *Journal of Sound and Vibration* 226 (3) (1999) 469–492.
[20] P. Goldman, A. Muszynska, Chaotic behaviour of rotor–stator systems with rub, *Journal of Engineering for Gas Turbines and Power—Transactions of the American Society of Mechanical Engineers* 116 (3) (1994) 692–701.
[21] R.D. Neilson, A.D.S. Barr, Dynamics of a rigid rotor mounted on discontinuously non-linear elastic support, *Institution of Mechanical Engineers* 202 (5) (1988) 369–376.
[22] E.V. Karpenko, M. Wiercigroch, M.P. Cartmell, Regular and chaotic dynamics of a discontinuously nonlinear rotor system, *Chaos, Solitons and Fractals* 13 (6) (2002) 1231–1242.
[23] E.V. Karpenko, M. Wiercigroch, E.E. Pavlovskaia, M.P. Cartmell, Piecewise approximate analytical solutions for a Jeffcott rotor with a snubber ring, *International Journal of Mechanical Sciences* 44 (3) (2002) 475–488.